FFI-RAPPORT

16/01483

MODITIC wind tunnel experiments

–

Alan Robins
Paul Hayden
Emma M. M. Wingstedt

MODITIC wind tunnel experiments

Alan Robins
Paul Hayden
Emma M. M. Wingstedt

Norwegian Defence Research Establishment (FFI) 13 October 2016

Keywords

EDA
Vindtunnel
Atmosfærisk turbulens
Eksperimentelle metoder
Gassutslipp
Spredning

FFI-rapport
FFI-RAPPORT 16/01483

Project number
1392

ISBN
P: 978-82-464-2822-2
E: 978-82-464-2823-9

Approved by
Hanne Breivik, *Research Manager*
Janet Martha Blatny, *Director*

Summary

The European Defence Agency (EDA) project B-1097-ESM4-GP “MOdelling the DIspersion of Toxic Industrial Chemicals in urban environments” (MODITIC) (2012 – 2016) has studied the release and transport of neutral and non-neutral chemicals in complex urban environments, in order to enhance the understanding of the dominating physical processes involved, and to support improvements in modelling techniques.

This report describes the MODITIC wind tunnel experiments in which the dispersion of non-buoyant (air) and heavier-than-air (carbon dioxide) emissions was investigated, both to provide detailed and extensive data sets for testing the performance of dispersion models and to investigate dense gas dispersion in complex topographical conditions.

The wind tunnel, instrumentation and scaling relationships are described, followed by summaries of the experimental work, which is divided into six categories:

1. A flat surface
2. A two-dimensional hill
3. A two-dimensional back-step
4. A simple array of obstacles
5. A complex array of obstacles
6. An urban area (central Paris).

The dispersion of both continuous and short duration emissions of air, carbon dioxide and air-carbon dioxide mixtures was investigated, in some cases with associated LDA (Laser-Doppler Anemometry) measurements of the velocity field. Concentrations were obtained with a single FFID (Fast Flame Ionisation Detector), except in a number of experiments in which four FFIDs were deployed. The latter experiments provided simultaneous concentration traces from four locations, giving data that can be used to examine the performance of inverse modelling techniques and their response to data quality. The whole data set is available as a collection of text and Excel files, with accompanying meta-data.

Sammendrag

European Defence Agency-prosjektet B-1097-ESM4-GP MODITIC (MOdelling the DIspersion of Toxic Industrial Chemicals in urban environments) har studert utslipp og spredning av nøytrale og ikke-nøytrale industrikjemikalier i urbane miljøer. Målene er både å øke kunnskapen om de dominerende fysikalske prosessene som er involvert og å støtte opp om forbedring av modelleringsteknikker.

Denne rapporten beskriver vindtunneleksperimentene som har blitt gjort i MODITIC, der spredning fra utslipp av nøytrale (luft) og ikke-nøytrale (karbondioksid) gasser ble undersøkt. Formålet med eksperimentene var både å samle detaljerte og omfattende datasett for å kunne sammenligne dem med resultatene fra spredningsmodeller og å undersøke tunggass-spredning i komplekse topografiske forhold.

Vindtunnelen, instrumenteringen og skaleringsforholdene er beskrevet, etterfulgt av sammendrag av det eksperimentelle arbeidet, som er delt inn i seks kategorier:

1. En plan overflate
2. En to-dimensjonal forhøyning
3. Et to-dimensjonalt bakvendt trinn
4. Et enkelt sett av kuber
5. Et komplekst sett av kuber
6. Et urbant område (sentrum av Paris).

Spredningen av både kontinuerlige og kortvarige utslipp av luft, karbondioksid og blandinger av disse to ble undersøkt, i noen tilfeller sammen med LDA-målinger (Laser-Doppler Anemometry) av hastighetsfeltet. Konsentrasjoner ble målt med en enkel FFID (Fast Flame Ionisation Detector), bortsett fra i enkelte eksperimenter der fire FFID-er ble utplassert. De sistnevnte eksperimentene gir samtidige konsentrasjonsmålinger fra fire ulike posisjoner, som kan brukes til å undersøke resultatene fra inverse modelleringsteknikker samt deres respons på datakvaliteten. Hele datasettet er tilgjengelig som en samling av tekst- og Excel-filer med tilhørende metadata.

Contents

Preface

This work is part of the European Defence Agency (EDA) project B-1097-ESM4-GP “Modelling the dispersion of toxic industrial chemicals in urban environments” (MODITIC). The scientific objective of this project is the systematic study of the release and transport of neutral and non-neutral chemicals in complex urban environments, to enhance understanding of the dominating physical processes involved, and to support improvements in modelling techniques. The participating organisations are:

- Direction Générale de l’Armement (DGA), DGA CBRN Defence, France
- Institut National de l’Environnement Industriel et des Risques (INERIS), France
- Norwegian Defence Research Establishment (FFI), Norway
- Swedish Defence Research Agency (FOI), Sweden
- University of Surrey (UoS), United Kingdom

FFI is the lead organisation. The project was initiated September 1, 2012, with a duration of three-and-a-half years. The project is funded by the Norwegian Ministry of Defence, the Swedish Ministry of Defence, the French Ministry of Defence, and the French Ministry of Ecology, Sustainability and Energy.

This report is authored by UoS and is published in FFI report series.

We also gratefully acknowledge the contributions to this work from staff at the University of Surrey, in particular: Paul Nathan, Matteo Carpentieri, Allan Wells, Ashley Nunn, Jack Benson and Joseph Batten.

1 Introduction

To somewhat paraphrase the project proposal:

> "The objective of the MODITIC project is to conduct a systematic study of the wind-borne transport of neutral and non-neutral gaseous chemicals in complex urban environments, so as to enhance understanding of the processes involved and support improvements in computational modelling techniques. The project will perform numerical simulations and wind tunnel dispersion experiments, together with experiments on chemical reactivity and environmental impact. An important outcome will be a database comprising the output from both the high fidelity numerical simulations and the wind tunnel experiments."

This report describes the latter, the wind tunnel experiments, which were undertaken in the EnFlo 'meteorological' wind tunnel at the University of Surrey, UK.

The EnFlo wind tunnel was designed specifically to simulate flow and dispersion processes in the atmospheric boundary layer, in particular where density differences are a key factor, either in emissions or the background flow. The key features of the tunnel that are a direct consequence of these requirements are a 20 m long working section, 3.5 by 1.5 m in cross-section, the capability to heat and cool the flow and the tunnel surfaces, and the ability to operate at low flow speeds. Relevant previous work includes the PERF project that studied dense gas dispersion in neutral and stable boundary layers ([1], [2]), the DAPPLE studies of dispersion in central London ([3]) and the DYCE project that investigated inverse modelling for identifying source location and strength ([4]).

MODITIC planning identified a number of scenarios of increasing complexity, the aim being to ensure gradual progress in complexity that, in turn, would lead to progress in understanding and capability, namely:

1. Flat surface
2. Two-dimensional hill
3. Two-dimensional back-step
4. Simple array of obstacles
5. Complex array of obstacles
6. An urban area (central Paris).

Each of these categories was then sub-divided to define boundary layer stability, wind direction, source properties and measurement requirements.

Chapter 2 describes the wind tunnel facility, discusses the similarity relationships between wind tunnel and full scale conditions, and sets out the modelling strategy, Chapter 3–8 describe the wind tunnel work for each category and Chapter 9 provides some final conclusions.

2 Wind tunnel modelling of dense gas dispersion

2.1 The EnFlo wind tunnel

The EnFlo wind tunnel commenced operation at the University of Surrey in 1993 and is the only such facility in the UK that is capable of simulating a range of atmospheric stabilities, rather than only neutral conditions. Its design specification was based on a perceived need in the middle and late 1980s for nuclear power station safety research. The key features of the tunnel are shown in Figure 2.1, they are:

- an open circuit 'suck-down' design,
- a simple inlet followed by a 15 layer inlet flow heater,
- a 20 m long working section comprising interchangeable 1 × 1.5 m panels, separate roof or floor heating and cooling panels, 3-zone heated wall panels (to minimise differences between wall and flow temperatures),
- two three-dimensional traverse systems, and
- twin fans, preceded by a heat exchanger to return the flow to ambient temperatures.

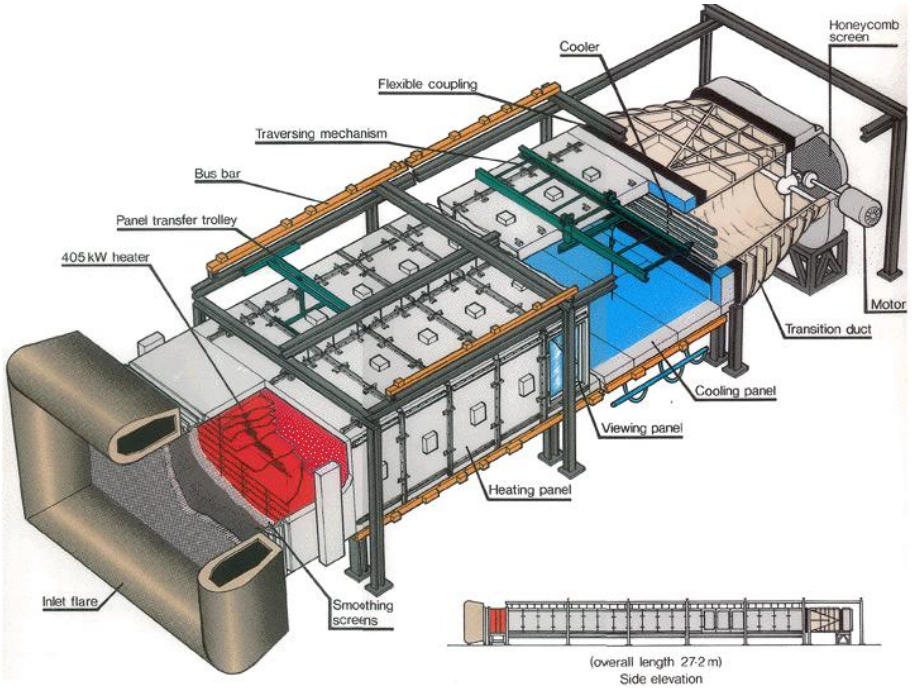

Figure 2.1 *Cutaway diagram of the EnFlo wind tunnel. The working section is 20 m long and the overall length 27.2 m. The technical specification is summarised in Table 2.1.*

Figure 2.2 shows a typical experimental set-up in which the tunnel's heating and cooling facilities are used, for example, to simulate stable or unstable flow conditions; heating and cooling are not required when the tunnel is operated in neutral stability conditions. The associated gas emission, sampling

Working section	
dimensions, m	$20 \times 3.5 \times 1.5$
overall length, m	27.2
flow speed range, ms^{-1}	0.3 to 3.0
Traverse equipment range	
longitudinally, m	5 to 20 (from entrance to working section)
laterally, m	-1.5 to +1.5
vertically, m	0 to 1.5
Inlet heater	
number of layers	15 @ 0.1 m deep
maximum heating rate, kW	400
maximum temperature gradient, Km^{-1}	80
Floor or roof panels	
unit size, m	1×1.5
maximum heating rate, kWm^{-2}	5
maximum surface temperature, K	120
maximum cooling rate, kWm^{-2}	1
minimum surface temperature, °C	~ 10

Table 2.1 *Technical specification of the EnFlo wind tunnel. The minimum surface temperature is limited by the dew point in the laboratory.*

and analysis systems are also shown, along with the tunnel control and condition monitoring equipment. Reference flow conditions are measured by two ultrasonic anemometers, one held at a fixed reference location and the other positioned as required; the motor shaft speed is also monitored. Temperature conditions are monitored by thermistor rakes in the flow and individual thermistors in each tunnel wall, roof and floor panel. Flow conditions through the inlet are also monitored, primarily to indicate the state of the inlet screens. The wind tunnel and associated experimental equipment operate under full computer control. This allows un-manned operation, overnight running in particular, and remote operation of the control software. All data collected, including a wide range of environmental and operational information and web-cam outputs, are automatically archived.

2.2 Experimental procedures

All velocity and turbulence measurements were made using a two-component Dantec Laser-Doppler Anemometer (LDA) system with a FibreFlow probe of outside diameter 27mm and focal length 160mm. This provided a measuring volume with a diameter of 0.074m and a length of 1.57mm. Data collection durations were selected to control the standard error in the results, achieving a typical standard error in the longitudinal mean velocity of about 2%, and in the turbulence normal stresses between 5 and 10%. Positional accuracy was generally ±2 mm, but locally better following reset of the traverse movement.

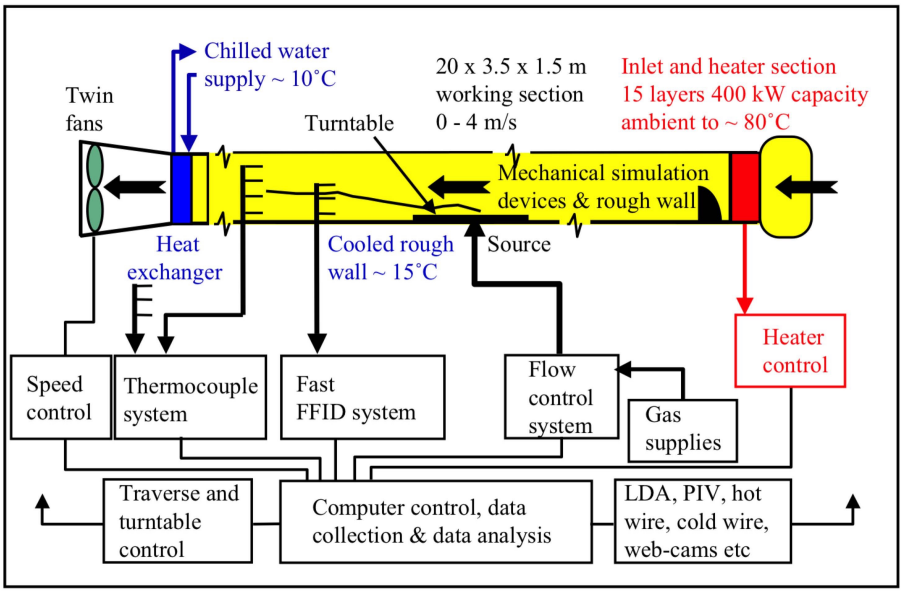

Figure 2.2 *Schematic diagram of the operation and control systems for the EnFlo wind tunnel and experimental equipment.*

Plume concentrations were determined with Cambustion Fast Flame Ionisation Detectors (FFID), which respond to hydrocarbon concentrations and have a frequency response of order 200 Hz. Small proportions of propane (of order 1%) were added to emissions and acted as the plume tracer, the precise concentration at the source being selected to ensure that the FFIDs operated within range. FFIDs were calibrated at regular intervals against standard mixtures of tracer-in-air. Data collection times were selected to control the standard error in the results; achieving a typical standard error of about 2% in the mean concentration (Quality A). In fact, two data qualities were adopted, Quality A with a 4 minute averaging time and Quality B with 1 minute. The first was used to determine the vertical and longitudinal spread of the plume between the source and the end of the measurement domain, the second was added to provide full cross-sectional mappings. As for the LDA, positional accuracy was generally ±2 mm, but locally better following reset of the traverse movement.

A standard source diameter of 0.1 m was used, the source installation extending to approximately 0.3 m below the tunnel floor and being packed with 3 mm diameter beads and covered with a mesh in order to achieve uniform emission conditions; similar arrangements were used in the PERF dense gas dispersion studies ([1]). In the majority of cases, emissions were either air or carbon dioxide with a trace amount of propane added, as discussed above. Mixtures of air and carbon dioxide were used in some experiments with the Paris model to obtain intermediate densities. A thermal mass-flowmeter and regulator system was used to control and monitor emissions.

2.3 Similarity considerations

The simulation conditions for modelling atmospheric dispersion in a wind tunnel are well established (e.g. [5],[6]). The main requirements are summarised here.

2.3.1 Boundary layer simulation

Similarity implies that all dimensionless profiles and boundary conditions of the undisturbed boundary layer are the same at model and full scale. An important constraint for a simulation to be valid is that the roughness Reynolds number, Re^*, at model scale is sufficiently large to ensure fully turbulent conditions, namely that:

$$Re^* = \frac{u^* z_o}{\nu} > 1 \tag{2.1}$$

where u^* is the friction velocity, z_o the roughness length and ν the kinematic viscosity ([7]). A further Reynolds number requirement ensures that the flow around model buildings is independent of Reynolds number; this is generally expressed as ([8]):

$$\frac{U(h)h}{\nu} > 10000 \tag{2.2}$$

where h is the height of the building. This is only applicable to buildings with sharp edges that fix separation points, the flow around curved surfaces being particularly sensitive to Reynolds number. It follows that in neutral conditions there is no explicit relationship between the wind speed in the tunnel and that at full scale. This situation only lasts whilst there are no density differences in the flow, from either boundary layer stability or emission buoyancy

The ratio of the Monin-Obhukov length scale, L_{MO}, and the boundary layer depth, H, becomes the key similarity parameter in stable or unstable conditions, and this directly links the wind speeds and temperatures at model and full scale, as in (2.3).

$$L_{MO} = \frac{u^{*3}}{\kappa g S_o/T} = \frac{u^{*2}}{\kappa g \theta^*/T}$$
$$\frac{L_{MO}}{H} = -\frac{1}{\kappa}\frac{u^{*2}}{gH}\frac{T}{\theta^*}$$

and hence

$$\varepsilon_u = \frac{u_1^*}{u_2^*} = \left(\frac{H_1}{H_2}\frac{\theta_1^*}{\theta_2^*}\right)^{1/2} = (\varepsilon\varepsilon_\theta)^{1/2} \tag{2.3}$$

where κ is von-Karman's constant, g the acceleration due to gravity, S_o the heat flux at the surface, T the ambient temperature, θ^* the friction temperature (defined by $S_o = u^*\theta^*$) and the suffices '1' and '2' refer to the two scales (i.e. full scale and model); ε, ε_u and ε_θ are, respectively, the scale ratios for geometry, speed and temperature.

2.3.2 Emission modelling

Scaling of the plume dynamics for inert emissions implies similarity of three parameters: a density ratio, a velocity ratio and a Richardson number, defined in (2.4). Strictly speaking there is also an emission Reynolds number to consider but it is assumed that this is sufficiently large for the phenomena of interest to be Reynolds number insensitive. The parameters are:

$$\frac{\rho_o}{\rho}, \frac{W_o}{u^*}, \frac{gD}{u^{*2}} \tag{2.4}$$

where ρ is density, W the vertical velocity and D the source diameter (U_{ref} can replace u^* and any suitable length scale can be used in place of D as there is no distortion to the geometry); the suffix 'o' denotes source conditions. This implies the following relationship between the speed and geometry scales:

$$\varepsilon_u = \frac{u_1^*}{u_2^*} = \frac{U_{ref1}}{U_{ref2}} = \left(\frac{D_1}{D_2}\right)^{1/2} = \varepsilon^{1/2} \tag{2.5}$$

where U_{ref} is a reference wind speed. This result stands alone when the dispersion takes place in a neutral boundary layer, otherwise (2.5) and (2.3) are only consistent when $\varepsilon_\theta = 1$. This is not a particularly comfortable situation for wind tunnel modelling as (2.5) implies that air speeds in a wind tunnel must be very low if realistic wind speeds in the atmosphere are to be simulated (given that ε is likely to be in the range from 1:100 to 1:300).

The conventional resolution to this problem is to relax the strict similarity conditions expressed by (2.4) by arguing that the density ratio is only important in defining buoyancy forces (akin to the Boussinesq approximation) and that the three parameters can be combined into two, a dimensionless emission buoyancy flux and a dimensionless emission momentum flux (see [5] and Appendix A). Exaggeration of the density difference in the wind tunnel simulation leads to an improvement on (2.5). This approach was not feasible in the present work as the only suitable, low-cost, heavier-than-air gas was carbon dioxide, which is actually less dense than many of the substances of interest at full scale.

2.3.3 Time

Times, t, at model and full scale are related through the dimensionless parameter, tU_{ref}/H, leading to a scale ratio for time, ε_T, where:

$$\varepsilon_T = \frac{t_1}{t_2} = \frac{H_1}{H_2}\frac{U_{ref2}}{U_{ref2}} = \varepsilon\varepsilon_u^{-1}. \tag{2.6}$$

As noted above, ε_u is arbitrary in flows without buoyancy effects; i.e. it is not defined by the scaling conditions.

2.3.4 Concentration

2.3.4.1 Steady emissions

The dimensionless concentration, C^*, used to convert concentrations at one scale to those at another, is defined as:

$$C^* = \frac{CU_{ref}H^2}{Q} \tag{2.7}$$

where consistent units are used for the emission rate, Q, and the concentration, C; i.e. volume or mass concentrations with volume of mass emission rates. Some care is necessary when working with volume concentrations in this way when there is a significant temperature difference between the emission and its environment. The volume emission rate is usually defined as $(\pi/4)D^2W_o$ but the appropriate value for making concentrations dimensionless will usually be that at the ambient temperature.

2.3.4.2 Short duration and unsteady emissions

There are many examples where ensemble measures replace time averages because of the unsteady nature of source terms. For present purposes, a short release is taken to be one for which the time of flight, T, is much greater than the release duration, ΔT. The plume limit is $\Delta T/T >> 1$ and the puff limit $\Delta T/T << 1$. The release rate, Q, is the appropriate measure for forming dimensionless concentrations in a plume, whereas in a puff it is the total amount released, M (in either volume or mass units). In the latter case, dimensionless concentrations are formulated as:

$$C_m^* = \frac{CH^3}{M} \tag{2.8}$$

and again C and M are expressed in consistent units. For a finite duration emission M can be written as $Q\Delta T$ and then:

$$C_m^* = \frac{CH^3}{Q\Delta T} = \frac{CUH^2}{Q}\frac{H}{U\Delta T} = \frac{H}{U\Delta T}C^* \tag{2.9}$$

defining the correspondence between the two forms of dimensionless concentration.

2.4 Modelling strategy

The scenarios of interest to the MODITIC project group were based on feasible though large emissions of hazardous materials as clouds that are heavier than air. However, what could be simulated in the wind tunnel work was tempered by the constraints of the simulation criteria discussed above, which are particularly severe in the case of dense gas dispersion modelling. The wind tunnel work therefore adopted a different strategy, namely to use experimental conditions, controlled by the tunnel speed, U_{ref}, and the emission rate of carbon dioxide, Q, that led to clear dense gas effects. A further constraint was that dispersing plumes remained well clear of the wind tunnel side walls. Thus in each of the six categories defined above, initial experiments were conducted to set the appropriate range for U_{ref} and Q before proceeding to the main set of experiments.

The data obtained in this manner can be used to test models that operate satisfactorily at model scale, in particular CFD-based approaches. However, some operational models can only be run at full scale and for these the similarity conditions described above were used to convert results from model to full scale. This generally led to emission conditions that were out of range for the applicability of operational models (emissions being far too large). Additional experiments were consequently carried out with reduced emission rates and tunnel speeds to provide data for more realistic full scale conditions, accepting that dense gas effects might be much reduced in such circumstances.

2.5 The approach flow

A neutrally stable approach flow boundary layer was simulated in a standard manner with Irwin spires and surface roughness. Its characteristics (the mean velocity, Reynolds stresses and length

scale profiles) are given in Appendix B and in greater detail in [9]. The boundary layer depth, roughness length, friction velocity and roughness Reynolds number are:

$$
\begin{aligned}
&H = 1 \text{ m} \\
&z_o = 0.8 \text{ mm} \\
&u^*/U_{ref} = 0.055 \\
&Re^* = 2.9 \text{ at } U_{ref} = 1 \text{ ms}^{-1}.
\end{aligned}
\tag{2.10}
$$

The region over which dispersion was studied was generally left smooth. This was done to avoid the need to simulate roughness elements in CFD simulations. A number of experiments were repeated with and without the omitted roughness elements in place and no significant differences were observed in plume dispersion behaviour.

3 Category 1: The flat surface

The work previously carried out during the PERF project provided sufficient data to satisfy the requirements for dense gas dispersion over a flat surface ([1, 2, 10]). A database was compiled from the results of the experiments at EnFlo covering the cases defined in Table 3.1. This was made available together with an index and associated PERF project reports as the database PERF-MODITIC.

Boundary layer stability	**Source type**	**Richardson number range**	**Measurements**
Dispersion measurements			
Neutral	Line	Ri^*_L = 0 to 55	Ground level and vertical concentration profiles.
Stable	Line	Ri^*_L = 1 to 26	
Neutral	Circular	Ri^*_C = 1 to 80	
Stable	Circular	Ri^*_C = 11 to 89	
Flow field measurements			
Neutral and stable			Approach flow conditions – vertical profiles of mean flow and turbulence.
Neutral	Line	Ri^*_L = 0 to 35	Vertical profiles of mean flow and turbulence.

Table 3.1 *Summary of the experimental conditions of the PERF-MODITIC database. The Richardson numbers Ri^*_L and Ri^*_C are defined in* (3.1)*.*

The Richardson numbers, Ri^*_L and Ri^*_C, as used in the PERF work are defined in (3.1).

$$Ri^*_L = \frac{g'_o q_o}{u^{*2} U_c}; \quad Ri^*_C = \frac{g'_o Q_o}{D u^{*2} U_c}; \quad g'_o = g\frac{\Delta\rho_o}{\rho} \tag{3.1}$$

where g is the gravitation acceleration, $\Delta\rho_o/\rho$ the fractional density difference of the emission, q_o the emission rate per unit source width of the line source, Q_o and D the total emission rate and diameter of the circular source, u^* the friction velocity of the approach flow and U_c the plume advection speed, defined as $U(z = d)$ with d the height of the roughness elements on the surface upstream of the source.

A second database, DYCE-MODITIC, was compiled from the results of the DYCE project ([4]) to provide data that could be used for initial MODITIC inverse modelling work. This contained two sets of data for the dispersion of passive emissions from a ground level point source in a neutral boundary layer, as summarised in Table 3.2. The first dataset enabled the ability to predict basic plume dispersion to be demonstrated, whereas the second dataset was for inverse modelling work. Fifteen minute concentration records were obtained in the latter experiments at a sampling rate of 400 Hz so that studies of the response of inverse modelling to data quality (e.g. averaging time and uncertainty) could be undertaken.

Dataset	Number of FFIDs deployed	Output	Purpose
Means	1	Mean concentration field	Fully define plume behaviour over the range of interest
15 minute time series, 2.5 ms sampling interval	4	Simultaneous concentration time series	Data for inverse modelling studies; 11 FFID configurations

Table 3.2 *Summary of the experimental conditions of the DYCE-MODITIC database.*

4 Category 2: The two-dimensional hill

The hill shape (tabulated in Appendix C) was scaled from the WALLTURB 'bump' ([11]), which itself was designed to generate a small separation bubble on the downwind face and for which high quality LES flow simulations had already been undertaken within the MODITIC group, albeit in a different context. The 0.3 m high hill was installed in the working section with its crest at 14.235 m from the section inlet; details of the installation are given in Figure 4.1. One source was located on the upwind slope, at 0.542 m from the crest, and another on the downwind slope, at 0.108 m from the crest. For practical reasons, both sources were located slightly to one side of the tunnel centreline, their centres at 0.125 m from the centreline. The hill span was 3.0 m and side walls were installed at $y = \pm 1.5$ m, as illustrated in the figure. Surface roughness was installed up to the leading edge of the model and downstream of its trailing edge, the hill itself being smooth.

Initial work extensively tested the similarity conditions, and the influence of the approach flow, surface conditions (i.e. roughness) and emission characteristics on plume behaviour, to guide the choice of preferred conditions for the main set of measurements. This led to the operational conditions summarised in Table 4.1, which for the case of carbon dioxide emissions produced significant heavy gas effects, namely greatly enhanced lateral plume spread, though free of any influence from the confines of the tunnel side walls. The Richardson number shown in the table, Ri^*, is defined in (4.1):

$$Ri^* = \frac{g'_o Q_o}{Du^{*2} U_c}; \quad g'_o = g\frac{\Delta\rho_o}{\rho}; \quad U_c = \frac{1}{2}U_{ref} \tag{4.1}$$

4.1 Results

A two component LDA and a FFID were mounted on the tunnel traverse system and used to measure vertical and lateral profiles of the velocity and concentration fields over and downwind from the hill. Both Quality A and B data were collected, the Quality A comprising vertical and longitudinal profiles though plumes at a number of locations between the source and the end of the

Source	**Emission**	**Emission rate Q, litre min^{-1}**	**U_{ref} ms^{-1}**	**Richardson number Ri***	**Emission speed ratio W_o/u^***
Upwind	air	100	1	0	3.9
Downwind	air	100	1	0	3.9
Upwind	CO_2	100	1	68	3.9
Downwind	CO_2	100	1	68	3.9

Table 4.1 *Experimental conditions used with the two-dimensional hill. The Richardson number, Ri^*, is defined in* (4.1)*.*

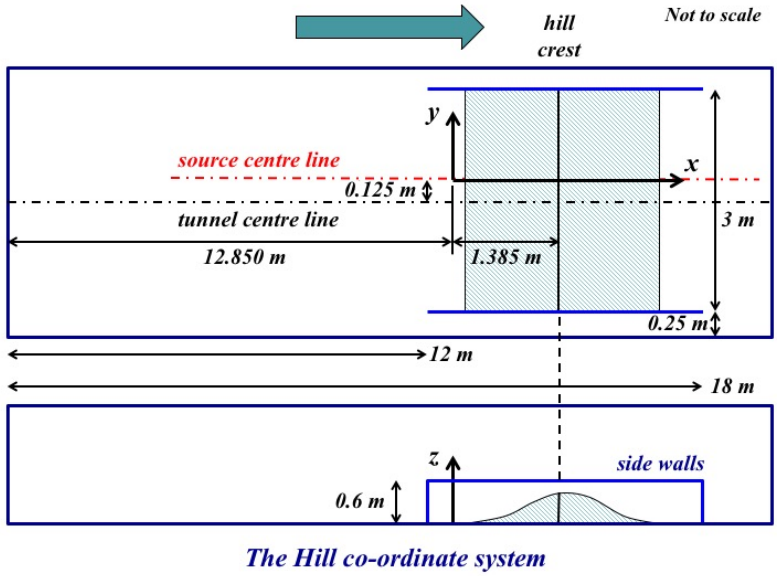

(a) Installation in the working section

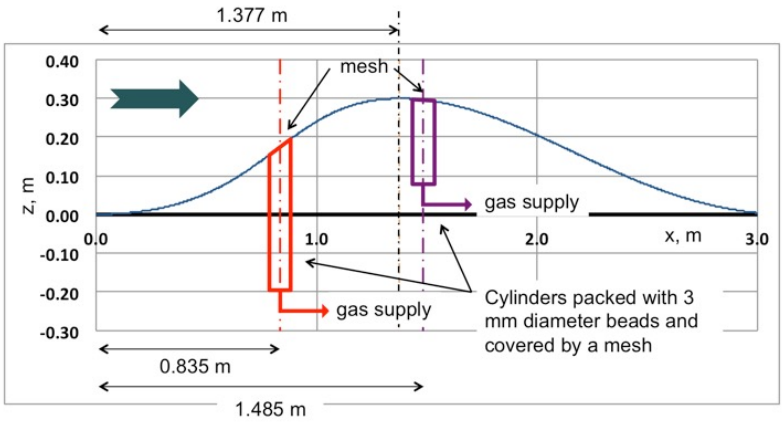

(b) The hill shape and source details

Figure 4.1 *General arrangement of the two-dimensional hill in the wind tunnel; source diameter 0.1 m. Location of the upwind source is shown in red and the downwind source is shown in purple.*

x, m	Quality A	Quality B	x, m	Quality A	Quality B
Upwind source (at x = 835 mm)			Downwind source (at x = 1485 mm)		
1050	X		1600	X	
1200	X		1750	X	
1400	X	X	1900	X	
1600	X		2050	X	X
1750	X		2200	X	
2050	X	X	2350	X	X
2350	X		2700	X	
2700	X		2850	X	
3000	X	X	3000	X	X
4000	X	X	4000	X	X

Table 4.2 *Measurement programme for Quality A and B data. The co-ordinate system is defined in Figure 4.1.*

measurement domain (x = 4.0 m in the co-ordinate system defined in Figure 4.1), and the Quality B data comprising full cross-sectional mappings at four of these locations. The details are given in Table 4.2.

The upwind source was located at x = 0.835 m. Strong dense gas effects were observed near the source where the mean flow was upwards along the hill. Here, the vertical mean velocity and the turbulence intensity levels were much less in the dense gas plume than in the air plume. The dense gas plume was considerably broader and shallower than the air plume at all locations, with reduced levels of concentration fluctuations and vertical turbulent mass fluxes.

The downwind source was located at x = 1.485 m, just downwind from the crest of the hill (x = 1.377 m), and the dense gas emission led to much increased velocities in the plume over the downwind face of the hill. As for the upwind source, the dense gas plume was again much broader and shallower than the neutral density plume and the reduced vertical spreading rate was reflected in lower vertical turbulent mass fluxes.

5 Category 3: The two-dimensional back-step

The back-step was formed by removing the downwind section of the hill model, separating the two parts at the crest. This however gave a step aspect ratio (width, Δy, to height, h) of just 10, which was clearly too small as it implied that the length of the recirculation region, L_R, formed downwind of the step was similar in magnitude to the step width (3 m). The floor level downwind of the step was built-up to reduce the step height to 0.1 m, increasing $\Delta y/h$ to 30 and implying that $\Delta y/L_R \sim 5$. The arrangement is shown in Figure 5.1. The source is located with its centre 0.1 m from the step. Experiments were conducted with the floor downwind of the step either smooth or covered in the roughness elements that were used to simulate the approach flow boundary layer. The programme of measurements is outlined in Table 5.1. The experimental conditions corresponded to $Ri^* = 0$ (air) or 68 (carbon dioxide) and $W_o/u^* = 3.9$.

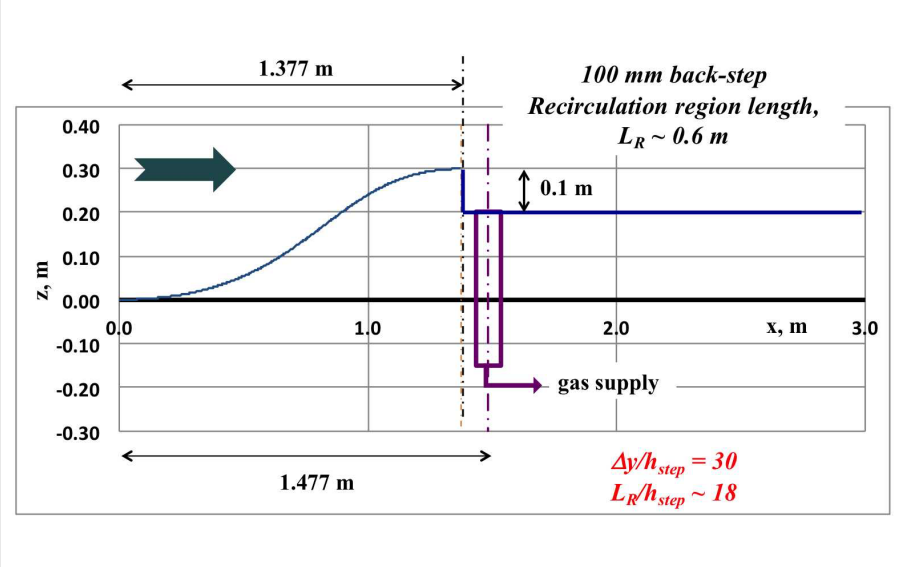

Figure 5.1 *General arrangement for experiments with the back-step. Source location is shown in purple.*

The most dramatic results were seen in the mean concentration field. In comparison with the neutral density plume, the heavier than air plume was much shallower, as expected, but essentially two-dimensional over the lateral extent investigated because lateral spread in the reversed flow near the source was very rapid, mixing the plume across the full width of the flow. Vertical turbulence intensities were much smaller in the dense gas plume and associated vertical mass fluxes greatly reduced, in keeping with the reduced rate of vertical spread. Differences between results over the smooth and rough wall were very small.

5.1 The two-dimensional back-step and obstacle array

Variants on the basic experiments with the back-step were achieved by installing arrays of obstacles on the downstream surface. These comprised three aligned rows of 0.11 m cubes spanning the full

Emission	Emission rate Q, litre min^{-1}	U_{ref} ms^{-1}	x, m	Profiles	
				Vertical	Lateral
Rough floor					
Neutral and heavier than air	100	1.0	1750	X	X
			2050	X	X
			2350	X	X
			2850	X	X
			3500	X	X
			4000	X	X
No emission		1.0	1050 to 4000	15	5
Smooth wall					
Neutral and heavier than air	100	1.0	1750	X	X
			2050	X	X
			2350	X	X
			2850	X	X
			3500	X	X
			4000	X	X

Table 5.1 *Velocity and concentration field measurement programme for the two dimensional back-step; the co-ordinate system is defined in Figure 4.1.*

width, separated laterally and longitudinally by 0.11 m. In the first case (Figure 5.2a), the obstacle array commenced at $x = 2.177$ m, 0.8 m from the step and downstream of the recirculation region; in the second (Figure 5.2b) at $x = 1.737$ m, well within the recirculation region. The programme of velocity and concentration field measurements is outlined in Table 5.2. As might be expected, the flow field within and downstream of the arrays showed a lateral structure comprising a series of obstacle wakes. However, the overall effect on dispersion was relatively mild, particularly in the case of the dense gas emissions because of rapid lateral mixing in the recirculating flow behind the step.

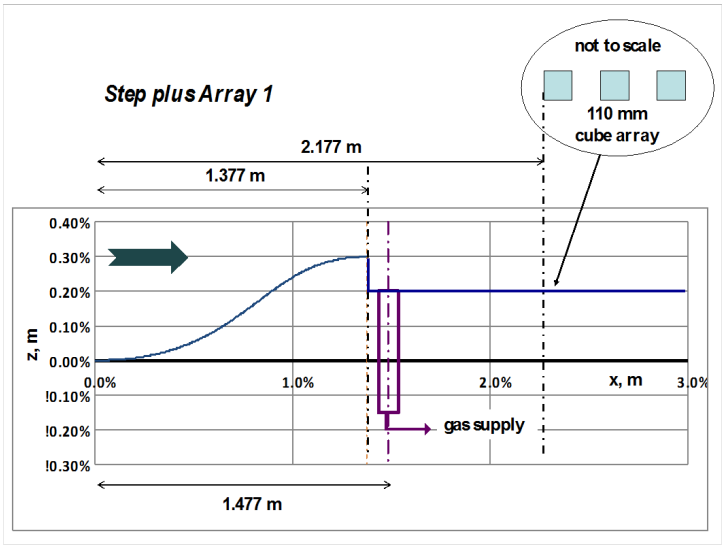

(a) Array 1

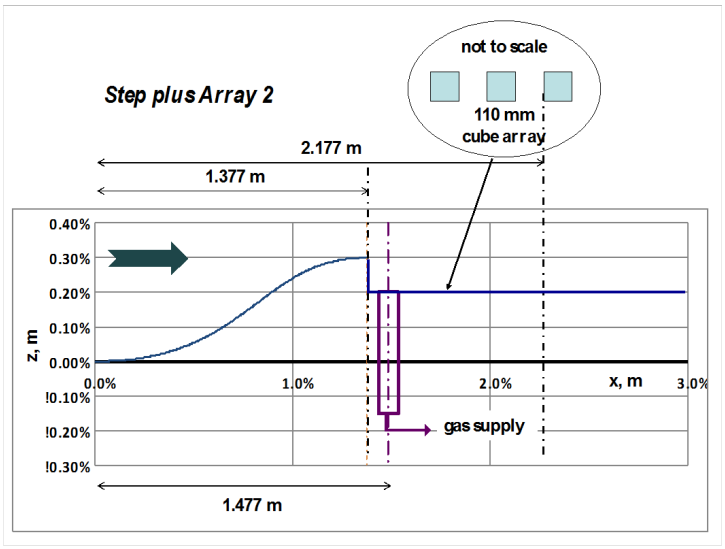

(b) Array 2

Figure 5.2 *General arrangement for experiments with the back-step and obstacle arrays. The source location is shown in purple.*

Emission	Emission rate Q, litre min^{-1}	U_{ref} ms^{-1}	x, m	Profiles	
				Vertical	Lateral
Array 1, commencing at x = 2.177 m					
Neutral and heavier than air	100	1.0	1750	X	X
			2050	X	X
			2350	X	X
			2570	X	X
			2850	X	X
			3500	X	X
			4000	X	X
No emission		1.0	3500	X	
			4000	X	
Array 2, commencing at x = 1.737 m					
Heavier than air	100	1.0	1910	X	
			2130	X	X
			2350	X	X
			2570	X	
			2850	X	
			3500	X	
			4000	X	

Table 5.2 *Measurement programme for the two dimensional back-step with a downstream obstacle array; the co-ordinate system is defined in Figure 5.2.*

6 Category 4 and 5: Single FFID data from the small and complex arrays

6.1 Category 4; the small array

The small array comprised four cubes of height $h = 110$ mm in a 2×2 array, with a separation of 110 mm. Experiments were carried out with the array either aligned normal to the approach flow, defined as 0°, or at 45°. Sources were located upwind, on the centre-line (S2, S3), or to one side at $y = 1.5h$ (S1). The general arrangements are shown in Figures 6.1a for the 0° orientation and 6.1b for the 45° orientation, and the experimental programme is summarised in Table 6.1. Three experiments were carried out to quantify any differences in basic dispersion behaviour over smooth and rough surfaces, the remaining five with the array in place.

Initial tests with source S2 and the array at 0° examined the effect of carbon dioxide emission rate on the plume width downwind of the array. The plume was judged to be too wide relative to the tunnel cross-section with a release rate of 100 litre min^{-1}, the value used with the hill experiments, and a lower emission rate of 50 litre min^{-1} was therefore adopted in this work and also that with the complex array. The experimental conditions corresponded to $Ri^* = 0$ (air) or 34 (carbon dioxide) and $W_o/u^* = 2.0$. The most obvious difference between the air and carbon dioxide plumes was that the former passed through the array whilst the latter were largely deflected around it.

6.2 Category 5; the complex array

An image of the complex array installed in the wind tunnel is shown in Figure 6.2. The basic model comprised fourteen rectangular blocks of differing sizes arranged in an irregular manner, all constructed from cubes of side $h = 110$ mm. The configuration shown in the figure included 'tree' simulators that were used in some of the experiments to study their impact on dispersion behaviour – this aspect is dealt with in Section 6.2.1. The array was aligned either normal to the approach flow, defined as 0°, or at 45°. The general arrangement is shown in Figure 6.3 for the 0° orientation; the model was rotated clockwise to the 45° orientation (i.e. the wind direction rotated through 45° anti-clockwise). Sources were located within the array (S1) at the origin, upwind on the centre line (S2) or to one side at $y = 3h$ (S3). The programme is summarised in Table 6.2. The experimental conditions corresponded to $Ri^* = 0$ (air) or 34 (carbon dioxide) and $W_o/u^* = 2.0$.

6.2.1 Category 5; the complex array with trees

There are no generally accepted methods for realistically modelling the aerodynamic effects of trees at small scale in a wind tunnel, particularly when located in urban streets. Nevertheless, a series of experiments was carried out to illustrate the potential impact of trees in an urban setting. Three different tree simulators were used, as defined in Figure 6.4. The first (disc) comprised two solid disks set at right angles to each other and mounted on a relatively thick support, the second (mesh)

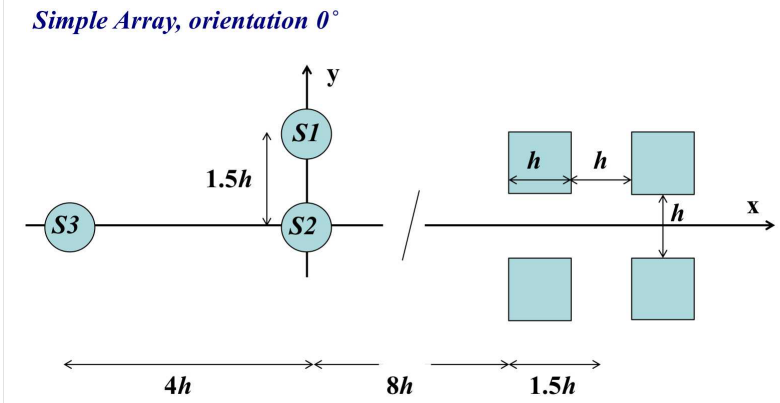

(a) 0°

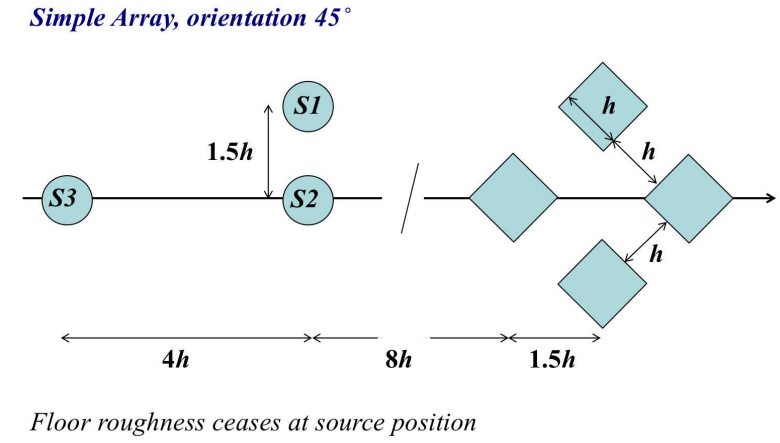

(b) 45°

Figure 6.1 *General arrangement for experiments with the small obstacle array.*

Orientation, degs	Source	Emission		U_{ref} ms^{-1}	x m
		Gas	Rate, Q litre min^{-1}		
No model, rough	S2	Air	50	1.0	500 to 4000 – 7 stations
No model, smooth	S2	Air			750 to 3000 – 6 stations
No model, smooth	S2	CO_2			
0	S1	Air			
45	S1	Air			
45	S1	CO_2			
0	S2	Air			
0	S2	CO_2			

Table 6.1 *Measurement programme for the small array; the lay-out is defined in Figures 6.1a and 6.1b. Vertical and lateral profiles of the flow and concentration fields were obtained at each station*

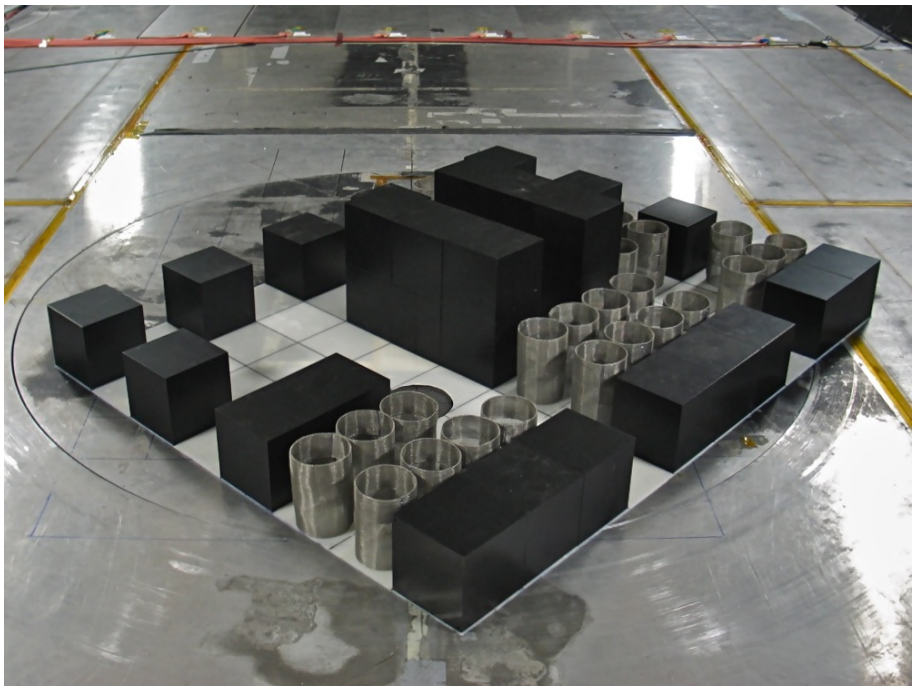

Figure 6.2 *Photograph of the complex array installed in the EnFlo wind tunnel.*

No trees Orientation, degs	Source	Emission		U_{ref} ms^{-1}	x m
		Gas	Rate, Q litre min^{-1}		
0	S1	Air	50	1.0	800, 1000, 1500, 2000, 3000
0	S1	CO_2			
0	S2	Air	50	1.0	-380, 55, 870, 1620, 1620
0	S2	CO_2			
0	S3	Air			
0	S3	CO_2			
45	S1	Air	50	1.0	800, 1000, 1500, 2000, 3000
45	S1	CO_2			

Table 6.2 *Measurement programme for the complex array without trees; the lay-out is defined in Figure 6.3. Vertical and lateral profiles of the flow and concentration fields were obtained at each station. The x locations for S2 and S3 are equivalent to 500, 935, 1750, 2500 and 3500 mm from the source positions.*

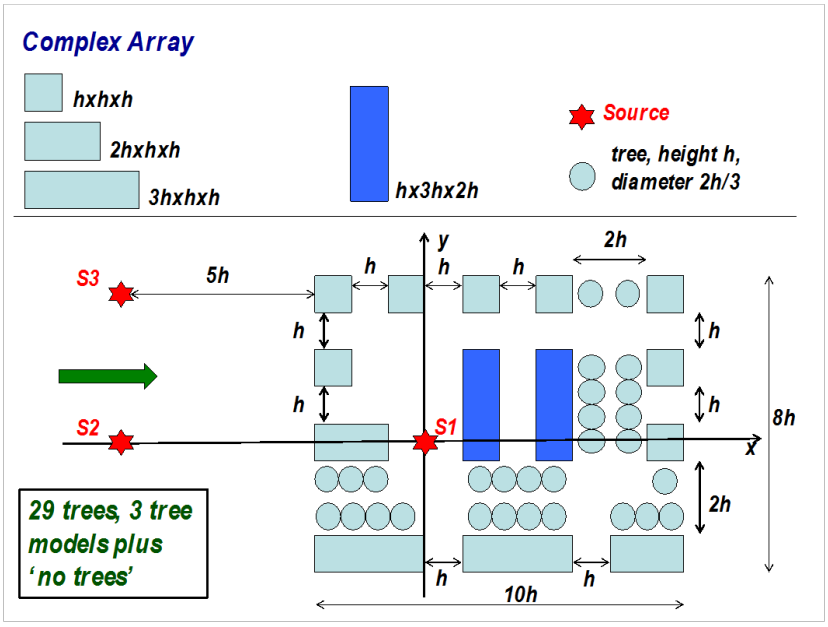

Figure 6.3 *General arrangement for experiments with the complex obstacle array.*

was based on a system developed at the University of Hamburg ([12]) and constructed from wire mesh, and the third (wool) comprised a sphere, more or less, of wire wool mounted on a slender support. All were 110 mm in height, the same as the height of the cubes used to construct the model. When installed, the discs of the first model were aligned at 45° to the adjacent building.

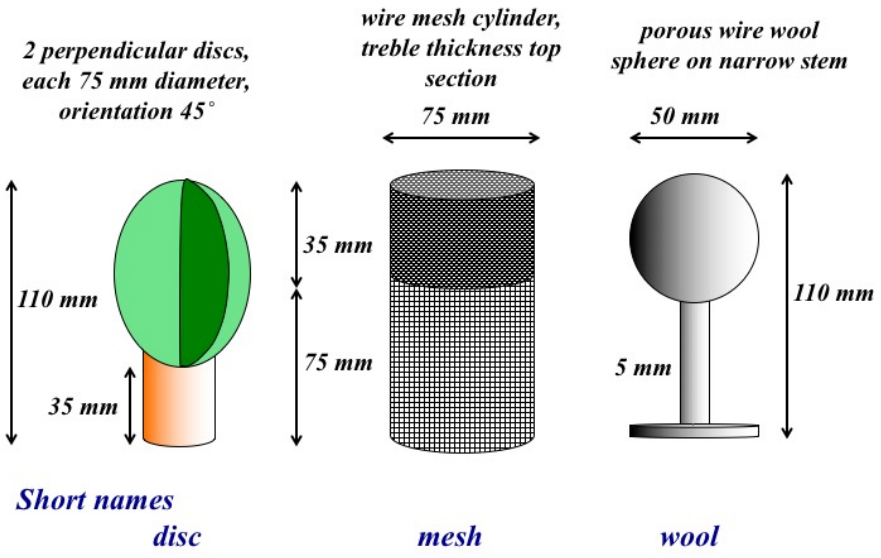

Figure 6.4 *Details of the three tree simulators.*

The aerodynamic characteristics of the three models were investigated by carrying out wake traverses with the simulators mounted on the wind tunnel floor in the undisturbed approach flow. All three were installed, side-by-side, with a lateral separation of $2h$ and vertical and lateral flow field traverses made at locations h upwind and $0.5h$, h and $2h$ downwind. The vertical profiles were obtained on the centre-line of each simulator. Equivalent data were recorded without the simulators in place.

The programme of plume dispersion studies is summarised in Table 6.3. Experimental conditions corresponded to $Ri^* = 0$ (air) or 34 (carbon dioxide) and $W_o/u^* = 2.0$. Most experiments used the mesh simulators but those with source S2 enabled a comparison to be made between the effects of all three tree simulators. The influence of the simulators on plume dispersion was most obvious in experiments with heavy gas emissions, where their presence led to some significant local changes in concentration levels. Of the three simulator types, the mesh produced by far the greatest changes.

Orientation degs	Tree type	Source	Emission		U_{ref} ms^{-1}	x m
			Gas	Rate, Q litre min^{-1}		
0	Mesh	S1	Air	50	1.0	800, 1000, 1500, 2000, 3000
0	Mesh	S1	CO_2			
0	All	S2	Air	50	1.0	-380, 55, 870, 1620, 1620
0	All	S2	CO_2			
45	Mesh	S1	Air	50	1.0	800, 1000, 1500, 2000, 3000
045	Mesh	S1	CO_2			

Table 6.3 *Measurement programme for the complex array with the tree simulators described in Figure 6.4; the overall lay-out is defined in Figure 6.3. Vertical and lateral profiles of the flow and concentration fields were obtained at each station. The x locations for S2 are equivalent to 500, 935, 1750, 2500 and 3500 mm from the source position.*

7 Category 4 and 5: Four FFID data from the small and complex arrays

Four FFIDs were operated simultaneously in these experiments to generate long data series that could be used for inverse modelling studies, in much the same manner as described for the DYCE-MODITIC data in Chapter 3. Experiments ran for 16 minutes, with the emission initially off, then on and, finally, off again so that concentrations fell to background levels by the end of the whole period, providing a period of approximately 13 minutes of steady emission. With this data set it was therefore possible to test the ability to detect the location of the source and the emission profile. Both the raw data, sampled at 400 Hz, and equivalent full scale data were made available, with conversion following the similarity considerations discussed in Section 2 and, for convenience, summarised again below.

Scaling of the dynamics of dense gas plumes implies similarity of three parameters: the emission density ratio, ρ_o/ρ, the emission velocity ratio, W_o/u^*, and the emission Richardson number,gD/u^{*2}, where the suffix 'o' denotes source conditions. This implies that the emission density ratio is the same at both scales and the relationship between the speed and geometry scales is:

$$\frac{U_{wt}}{U_{fs}} = \frac{W_{owt}}{W_{ofs}} = \varepsilon^{1/2} \tag{7.1}$$

where the suffices denote wind tunnel and full scale, and ε the geometrical scale ratio. The volume emission rates, Q, are related by:

$$Q_{fs} = Q_{wt}\varepsilon^{-5/2} \tag{7.2}$$

time through:

$$t_{fs} = t_{wt}\varepsilon^{-1/2} \tag{7.3}$$

and finally plume concentrations are related through the dimensionless variable C^*, defined in (2.7), implying that:

$$C_{fs} = C_{wt} \tag{7.4}$$

consistent units being used for the emission rate, Q, and the concentration, C.

A scale of $\varepsilon = 1/200$ was assumed in converting the results to full scale, the data being first down-sampled to 100 Hz. An arbitrary time origin was used to make the test of the inversion process more realistic. The converted data included the reference wind speed, model orientation and the location of the four detectors, followed by a list of time and volume concentrations (parts per thousand of the total emission) at each detector. The time interval was 144 ms.

7.1 Reference cases with no obstacles installed

Runs with the small array were preceded by four reference cases without any obstacles in place. In each of these, the emission was air, the emission rate 50 litre min^{-1} and the reference speed

Detector array name	Detector location (x, y, z) m			
Long	280, 0, 5	320, 0, 5	400, 0, 5	600, 0, 5
Span	400, -64, 5	400, -20, 5	400, 20, 5	400, 64, 5
Span + roughness	400, -64, 5	400, -20, 5	400, 20, 5	400, 64, 5
Square	400, -64, 5	400, 64, 5	600, -64, 5	600, 64, 5

Table 7.1 *Detector locations for the four experiments with no obstacles installed. At model scale the emission was air with $Q = 50$ litre min^{-1} and $U_{ref} = 1.0$ ms^{-1}. Locations are at full scale, assuming a scale ratio if 1:200. The origin is at the source.*

1.0 ms^{-1}. Table 7.1 specifies the arrangement of the FFID instrumentation, with the origin at the source. In the first array (Long) the detectors were aligned in the x direction, in the second (Span) in the y direction and in the third (Square) in a square array. The surface roughness ended at the source location in all but the case named "Span + roughness", where it continued downstream over the region where measurements were made.

7.2 Category 4; the small array

The same detector arrays were used in the experiments with the small obstacle array. Figure 7.1 specifies the geometry for these experiments, Table 7.2 the arrangement of the FFID instrumentation (all that has changed relative to Table 7.1 is the origin), and Table 7.3 the experiments carried out. Note that the origin is at the source location in all cases.

Detector array name	Detector location (x, y, z) m			
Long	280, 0, 5	320, 0, 5	400, 0, 5	600, 0, 5
Span	400, -64, 5	400, -20, 5	400, 20, 5	400, 64, 5
Square	400, -64, 5	400, 64, 5	600, -64, 5	600, 64, 5

Table 7.2 *Detector locations for the experiments with the simple obstacle array. Locations are at full scale, assuming a scale ratio if 1:200.*

Source	Orientation, degs	FFID array	Emission		Emission profile: off/on/off
			Air	CO_2	
S1	0	All	X		
S1	45	All	X	X	Approx. 3.5 hrs
S2	0	All	X	X	steady emission

Table 7.3 *Experimental conditions with the simple obstacle array. The source locations are defined in Figure 7.1.*

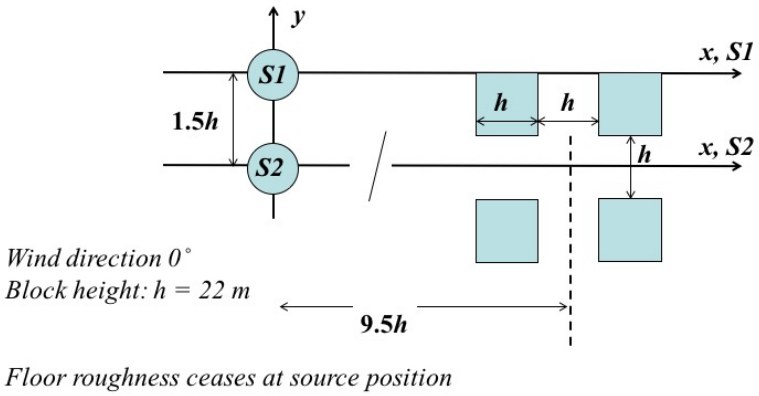

(a) 0° orientation

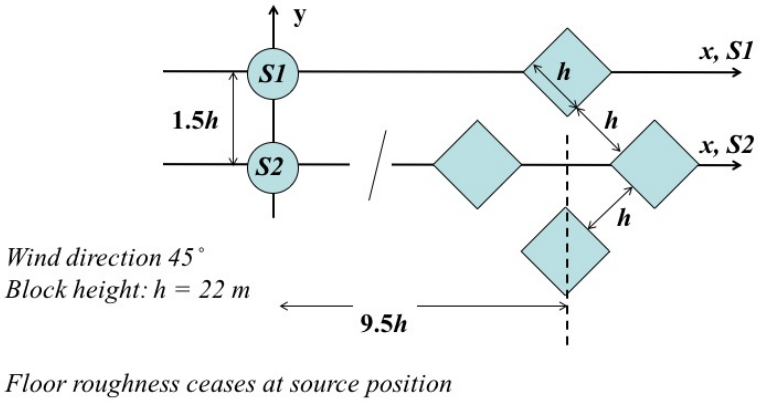

(b) 45° orientation

Figure 7.1 *General arrangement and origin definitions for experiments with 4 FFIDs and the small obstacle array at* 0° *and* 45° *orientations.*

7.3 Category 5; the complex array

The experiments with the complex obstacle array were somewhat different in that the FFID positions were all within the obstacle array, with some at roof level. Figure 7.2 specifies the geometry for these experiments, Table 7.4 the arrangement of the FFID instrumentation, using the co-ordinate system defined in the figure, and Table 7.5 the experiments carried out.

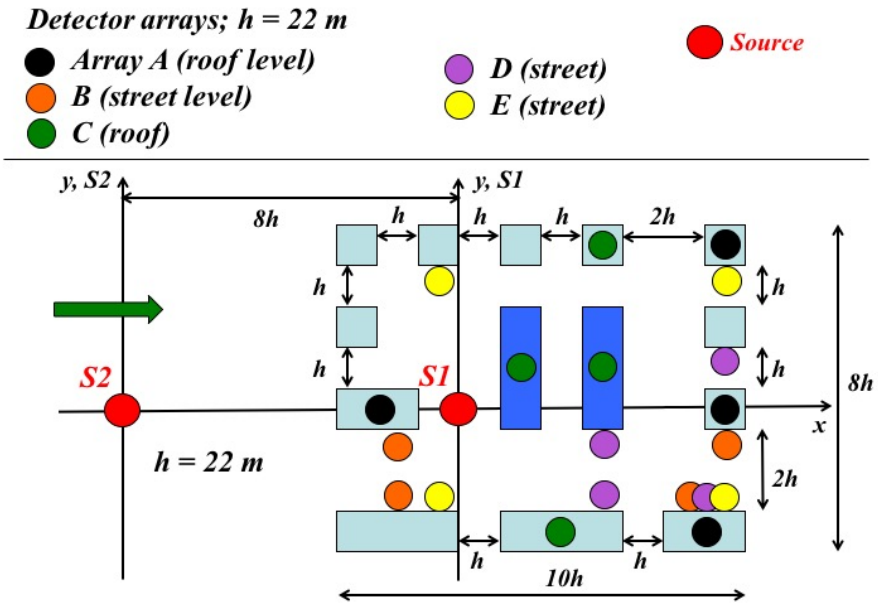

Figure 7.2 *General arrangement for experiments with 4 FFIDs and the complex obstacle array.*

Detector array name	Detector location (x, y, z) m			
A	-44, 0, 24	132, -66, 24	143, 0, 24	143, 88, 24
B	-33, -53, 2	-33, -13, 2	132, -53, 2	143, -13, 2
C	33, 22, 46	55, -66, 24	77, 22, 46	77, 88, 24
D	77, -53, 2	77, -13, 2	132, -53, 2	143, 31, 2
E	-11, -53, 2	-11, 75, 2	132, -53, 2	143, 75, 2

Table 7.4 *Detector locations for the experiments with the complex obstacle array. Locations are at full scale, assuming a scale ratio of 1:200 and an origin at Source S1.*

Source	Orientation, degs	FFID array	Emission		No trees installed
			Air	CO_2	
S1	0	C	X	X	Emission profile:
S1	0	D	X	X	off/on/off
S2	0	A	X	X	
S2	0	B	X	X	Approx. 3.5 hrs
S2	0	C	X	X	steady emission
S2	0	E	X	X	

Table 7.5 *Experimental conditions with the complex obstacle array. The source locations are defined in Figure 7.2. No tree simulators were installed for these runs.*

8 Category 6: An urban area (central Paris)

8.1 Continuous emissions

A model scale of 1:350 was selected in order to encompass a sufficient area of central Paris, from the Arc de Triomphe along Avenue des Champs Elysees to the Grand Palais, and an equivalent distance on either side. This made the scaling relationships for wind tunnel simulation, [(7.1),(7.2)], less favourable as the ratio of full scale and model wind speeds became $\sqrt{350} = 18.7$. The full extent of the wind tunnel model is shown in Figure 8.1 and an image of the model installed in the wind tunnel in Figure 8.2. The model comprised almost a hundred blocks, each with a flat roof, a great simplification of the real topography but one judged fit for purpose, given that whatever was used in the wind tunnel work had to be reproduced in the numerical modelling. One exception to the general procedure of simplification was the Arc de Triomphe, for which a reasonably realistic model was constructed.

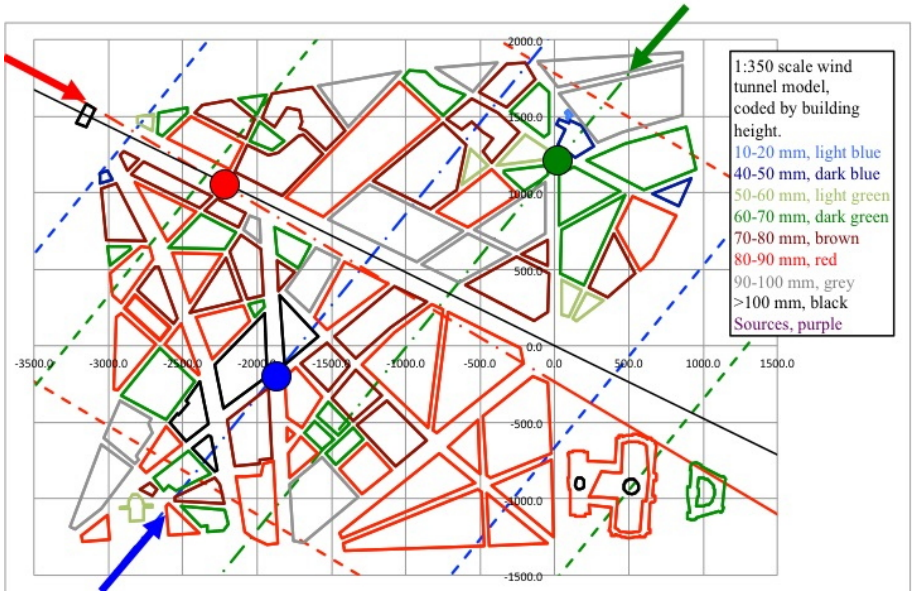

Figure 8.1 *Map of the 1:350 scale Paris model. The sources are shown as coloured circles and the associated wind directions marked in the same colours (red, S1; blue, S2; green, S3). The dashed lines denote the wind tunnel walls.*

Three source locations and associated wind directions were identified: one in the Avenue des Champs Elysees and two in the narrow side streets on either side. These are denoted by coloured circles in Figure 8.1. The expectation, justified by experience, was that the greater confinement in the latter two cases would have a significant impact on dispersion behaviour. A wind direction was associated with each source, as also shown in the figure: 300° for source 1, 220° for 2 and 40° for 3. In each case a wind-aligned co-ordinate system was used, with the origin at the source.

Three types of concentration measurements were made: in-street, lateral profiles (cross-wind) above roof level, at $z = 120$ mm, vertical profiles from street level. In distinct contrast with the

other scenarios, wide ranges of emission rates (1 to 50 litre min^{-1}), emission density ratios relative to air (1 to 1.52) and reference flow speeds (0.6 to 2.0 ms^{-1}) were examined. Further detail is provided in Table 8.1; note that in the upstream boundary layer $U(h)/U_{ref} = 0.62$, $U_{10}/U_{ref} = 0.48$, $u^*/U_{ref} = 0.055$, where h is the average block height (78 mm) and U_{10} is equivalent to the 10 m wind speed at full scale.

Figure 8.2 *Photograph of the 1:350 scale Paris model installed in the EnFlo wind tunnel.*

The experiments carried out for each of the three wind direction and source combinations is summarised in Tables 8.2, 8.3, and 8.4. In-street data were obtained at a height of 10 mm in the wind tunnel, equivalent to 3.5 m at full scale.

An emission rate of 50 litre min^{-1} and a reference speed of 1 ms^{-1} were used in the experiments with the simple and complex array and were the starting point for work with the Paris model. The dense gas effects were found to be very strong, with the carbon dioxide plume almost entirely confined to the street network and significant upwind and lateral spread apparent. A series of experiments was added to demonstrate the sensitivity of these observations to the emission conditions (density and flow rate) and wind speed. In all the cases studied, the downwind carbon dioxide plume was found to be much shallower than the equivalent air plume, though upwind spread ceased at sufficiently low emission rates. The runs with air at different emission rates produced concentration results that scaled with the emission rate, as expected of a passive plume with W_o/u^* fixed.

The relationships between conditions at model and full scale are discussed in Chapter 2.3.2 and imply, for example, that the ratio of full scale and model wind and emission speeds is $\sqrt{350} = 18.7$. Emission rates in the range from 35 to 50 litre min^{-1} were chosen to obtain pronounced dense gas effects at a tunnel reference speed of 1 ms^{-1}, the preferred minimum operating speed in terms of flow quality. Clearly, this combination translates to conditions that are unrealistic at full scale. The runs that were carried out with lower emission rates and reference wind speeds below 1 ms^{-1} were included to provide data in less-unrealistic conditions.

Emission	Emission rate, Q, litre min^{-1}	Density ration	U_{ref} ms^{-1}	Velocity ratio, W_o/u^*
Air	5	1	1.0	0.18
	10		1.0	0.36
	25		1.0	0.96
	35		1.0	1.35
	50		1.0, 2.0	1.39, 0.96
Air/CO_2 mixtures	4	1.25	1.0	0.15
	5	1.25		0.19
	50	1.10, 1.15, 1.20, 1.25, 1.30, 1.35 1.40		1.93
Carbon dioxide	1	1.52	1.0	0.04
	2		1.0	0.08
	2.5		1.0, 0.7, 0.8, 1.0	0.16, 0.14, 0.12, 0.10
	3		1.0	0.12
	4.7		1.0	0.18
	10		0.8, 1.0	0.48, 0.39
	14		1.0	0.54
	19		1.0	0.73
	25		1.0	0.96
	29		1.0	1.12
	34		1.0	1.31
	35		0.8	1.35
	38		1.0	1.47
	50		1.0, 1.25, 1.5, 1.8	1.93, 1.54, 1.29, 1.07

Table 8.1 *Experimental conditions used for concentration field measurements with the Paris model; source locations are defined in Figure 8.2; source diameter 0.1 m (model scale).*

Emission	Emission rate, Q, litre min^{-1}	U_{ref} ms^{-1}	Lateral profiles	Vertical profiles	In-street data
Air	3, 5, 25, 35, 50	1.0	4×17 point profiles at z = 120 mm, x =500, 750, 1000, 2000 mm	18×10 point profiles	~ 150 locations
Carbon dioxide (density ratio 1.52)	1, 2, 2.5, 3, 4.7, 10, 14, 19, 25, 29, 34 35, 38, 50	0.6, 0.7, 0.8, 1.0, 1.2, 1.5, 1.8		28×10 points profiles	~ 150 locations
Air–Carbon dioxide mixture (density ratio 1.1 to 1.25)	4, 5, 50	1.0		18×10 points profiles at x =1000 mm	

Table 8.2 *Experimental conditions for Source S1, wind direction* 300°

Emission	Emission rate, Q, litre min^{-1}	U_{ref} ms^{-1}	Lateral profiles	Vertical profiles	In-street data
Air	50,	1.0	4×17 point profiles at z = 120 mm, x =500, 750, 1000, 2000 mm	23×20 point profiles	~ 150 locations
Carbon dioxide (density ratio 1.52)	50	1.0		25×20 points profiles	

Table 8.3 *Experimental conditions for Source S2, wind direction* 220°.

Emission	Emission rate, Q, litre min^{-1}	U_{ref} ms^{-1}	Lateral profiles	Vertical profiles	In-street data
Air	25, 50,	1.0, 2.0	4×17 point profiles at z = 120 mm, x =500, 750, 1500, 2000 mm	28×20 point profiles	~ 150 locations
Carbon dioxide (density ratio 1.52)	25, 34, 38 50	1.0, 1.3			

Table 8.4 *Experimental conditions for Source S3, wind direction* 40°.

8.1.1 Comparison with DAPPLE experiments

DAPPLE dispersion experiments with passive emissions in central London showed a clear upper bound to the maximum dimensionless concentration at a given radius from a source and the dimensionless separation, R, which could be expressed as:

$$C^* = \frac{CU_{ref}^2 H^2}{Q} = 50\left(\frac{R}{H}\right)^{-2} \tag{8.1}$$

where H is any convenient height scale as it actually cancels from (8.1); see [3]. The data for air emissions from sources S2 and S3 were fully consistent with this result, but the data from S1 showed a much slower decay exponent, closer to -1, due to channelling of the flow and reduced lateral dispersion along Avenue des Champs Elysees. Behaviour of the dense gas plumes, as might be expected, did not follow (8.1) but could be fitted with a lower decay exponent. A series of experiments with S1 tested how the decay rate depended on plume Richardson number, showing a consistent decrease in the decay exponent with increasing stability.

8.2 Short duration emissions

A set of experiments with short duration emissions complemented those with continuous releases. Emission durations between 1 and 32 s were used at tunnel reference speeds between 0.8 and 1.0 ms^{-1}; the equivalent values at full scale being 19 to 600 s and 15 ms^{-1} ($U_{10} \sim 7$ ms^{-1}). The emission profile took the simple off-on-off form; measurements at the source showed the rise time of the concentration signal to be less than 0.5 s at a height of 5 mm and this was judged to be acceptable. About 50 repeat experiments were performed in order to provide a sufficient ensemble of results at each experimental condition, previous work having shown that this would be adequate for forming reliable statistics of the ensemble averaged concentration field. The delay between emissions in an ensemble was selected to ensure that concentrations returned to background levels.

Concentration data were collected from a single FFID at 400 Hz. Results from the ensembles were first of all scanned to identify and remove any corrupt cases; the first example in the ensemble was always rejected as this often proved to be atypical. Ensembles therefore contained 49 or slightly fewer examples. Tables 8.5 and 8.6 summarise the cases investigated.

There are two limits to the behaviour of a short duration emission, one the true puff where the travel time is large relative to the emission time, and the other where the emission time is large relative to the travel time. In the latter case, a clear plateau develops in the ensemble average concentration trace, where concentration levels are essentially the same as in the equivalent plume from a continuous release. Compared with the air plumes, a much longer emission duration, in some cases greater than 32 s, was required for the carbon dioxide plumes to attain this state. A related factor was the variation in upwind spread with release duration. The development of significant upwind spread was seen to be a function of the emission duration in situations that produced significant upwind spread from a continuous release.

The DAPPLE experiments ([3]) showed relatively well defined relationships between: a) plume advection speeds, deduced from arrival and departure times and the wind speed at roof level; b)

Emission	Emission rate, Q, litre min^{-1}	U_{ref} ms^{-1}	Emission duration, s	Data
Carbon dioxide	2	0.8	1, 2, 4, 8, 16, 32	3 locations, $z = 10$ mm
	2.5	0.8	2	4 locations, $z = 10$ mm
	10	0.8	1, 2, 4, 8, 16, 32	3 locations,$z = 10$ mm
	35	0.8	1, 2, 4, 8, 16, 32	3 locations,$z = 10$ mm
	35	1	1, 2, 4, 8, 16, 32	1 location,$z = 10$ mm
	35	0.8	2	12 locations,$z = 10$ mm
	35	0.8	1, 2, 4, 8, 16, 32	1 location,$z = 10, 25, 50, 75$ mm
Air	35	0.8	1, 2, 4, 8, 16, 32	3 locations, $z = 10$ mm

Table 8.5 *Short duration emissions from source S1.*

Emission	Emission rate, Q, litre min^{-1}	U_{ref} ms^{-1}	Emission duration, s	Data
Carbon dioxide	10	0.8	2	9 locations, $z = 10$ mm
	10	0.8	2	1 location, $z = 10, 36, 71, 106, 140$ mm
	35	0.8	2	8 locations,$z = 10$ mm
Air	35	0.8	2	10 locations, $z = 10$ mm

Table 8.6 *Short duration emissions from source S3.*

concentration rise and decay times in relation to the travel time. Similar relations were seen in the data from the Paris experiments with air plumes, though with greater scatter. In comparison, the behaviour of the dense gas plumes was very complex, with some cases showing prolonged rise and decay times. Overall, there was a very large degree of variation in the ratio of rise or decay time to travel time in these cases and no simple correlation was apparent.

9 Conclusions

A detailed and comprehensive data-base has been prepared from wind tunnel simulations of non-buoyant and dense gas dispersion in conditions of increasing geometrical complexity. The results were compiled as a set of text and Excel files, with accompanying geometry, approach flow and associated meta-data. The prime use of this data within the MODITIC project was to examine the performance of a range of forward and inverse dispersion models, though the results also provide insight into dense gas dispersion behaviour. Some of the models applied in MODITIC only accept input in full scale units and for these the wind tunnel data were converted to full scale values following the scaling relationships summarised in Chapter 2.3. In these cases, the data-base contains both the original data and that converted to full scale.

Experiments were also undertaken in stable boundary layers but results from these have not been included in the final data-base as the quality of the simulated stable boundary layers was judged inadequate. Significant improvements were subsequently made to the simulation system, making it possible to produce data of acceptable quality in stable flows. However, the wind tunnel time devoted to MODITIC work had already exceeded that planned by over 100% and additional work was not feasible.

One obvious follow-on study would be to benefit from the improvements in simulation techniques and repeat the work in stable boundary layers. Similar work could also be carried out in unstable boundary layers. Topics that deserve further and deeper study include the relation between upwind and lateral spread near the source and the emission properties (Richardson number and velocity ratio) and the adaptation of street network, urban dispersion models to dense gas emissions. These models use the entrainment velocity concept to represent the mixing between the flows in a street canyon and in the boundary layer above. How the entrainment velocity responds to stability resulting from density differences between the street canyon and boundary layer flows is not yet parameterised.

A Relaxed similarity conditions

The dimensionless emission buoyancy flux, F_B:

$$F_B = \frac{g'Q}{U^3 D} \tag{A.1}$$

arises in both plume rise and dense gas dispersion theory and is directly related to the source Richardson number defined in (4.1). A second parameter, F_M, derives from the emission momentum and is generally written in one of two ways:

$$F_M = \frac{W_o Q}{U^2 D^2}; \quad F_M = \frac{\rho_o W_o Q}{\rho U^2 D^2} \tag{A.2}$$

The argument that (A.1) and (A.2) form the basis for converting between wind tunnel and full scale leads to a modified form for the wind speed scale ratio:

$$\varepsilon_u = \frac{U_{fs}}{U_{wt}} = \varepsilon^{1/2} f\left(\alpha_{fs}, \alpha_{wt}\right); \quad \alpha = \frac{\rho_o}{\rho} \tag{A.3}$$

and an appropriate choice of the density ratio α_{wt} relative to α_{fs} improves on the speed scale ratio that is achieved when the two are equal (i.e. when $f = 1$). As an example, if the first of the two definitions for the momentum parameter is assumed, then:

$$\varepsilon_u = \frac{U_{fs}}{U_{wt}} = \varepsilon^{1/2} \left(\frac{\alpha_{fs} - 1}{\alpha_{wt} - 1}\right)^{1/2} \tag{A.4}$$

clearly showing the benefit accruing from setting $\alpha_{wt} >> \alpha_{fs}$; i.e. using a more dense gas at model scale. The procedure works well enough with lighter than air emissions ($\alpha_{wt} << \alpha_{fs}$), where helium can be used in wind tunnel work (e.g. see [5]), but benefits of (A.4) are not available to the MODITIC experiments as the gas used in the wind tunnel is carbon dioxide ($\alpha_{wt} = 1.52$) and most gases of practical interest are of greater density. It could though be applied to a fictitious case in which $\alpha_{wt} > \alpha_{fs} > 1$.

Both plume rise and dense gas dispersion theories indicate that the buoyancy parameter, (A.1), is the key concern when buoyancy effects dominate. In those situations, it can be said that this then becomes the only parameter linking model and full scale conditions, in which case:

$$\varepsilon_u^3 = \frac{1}{\varepsilon} \frac{(g'Q)_{fs}}{(g'Q)_{wt}} = \frac{1}{\varepsilon} \frac{((\alpha - 1)Q)_{fs}}{((\alpha - 1)Q)_{wt}} \tag{A.5}$$

taking the air density to be the same at both scales. Note that (A.4) is recovered if the emission speed ratio is set to the wind speed ratio. A more convenient form of (A.5) is:

$$\varepsilon_u^2 = \varepsilon \left(\frac{\alpha_{fs} - 1}{\alpha_{wt} - 1}\right) \frac{(W_o/U)_{fs}}{(W_o/U)_{wt}} \tag{A.6}$$

showing how combinations of emission density and velocity ratio can lead to an improvement on (A.3) with $f = 1$; basically, this requires:

$$\left(\alpha_{fs} - 1\right) \left(\frac{W_o}{U}\right)_{fs} < (\alpha_{wt} - 1) \left(\frac{W_o}{U}\right)_{wt} \tag{A.7}$$

which implies a large reduction in the emission speed ratio, W_o/U, at full scale relative to wind tunnel scale, given $\alpha_{fs} > \alpha_{wt}$.

B The approach flow characteristics

Full tabulations of the incoming flow conditions at 12.850 m from the working section entrance are provide in the spreadsheet: 'Undis_BL analysis.xlsx'.

The friction velocity, u^*, roughness length, z_o, and boundary layer depth, H, are:

H	1 m
u^*/U_{ref}	0.055
z_o	0.8 mm

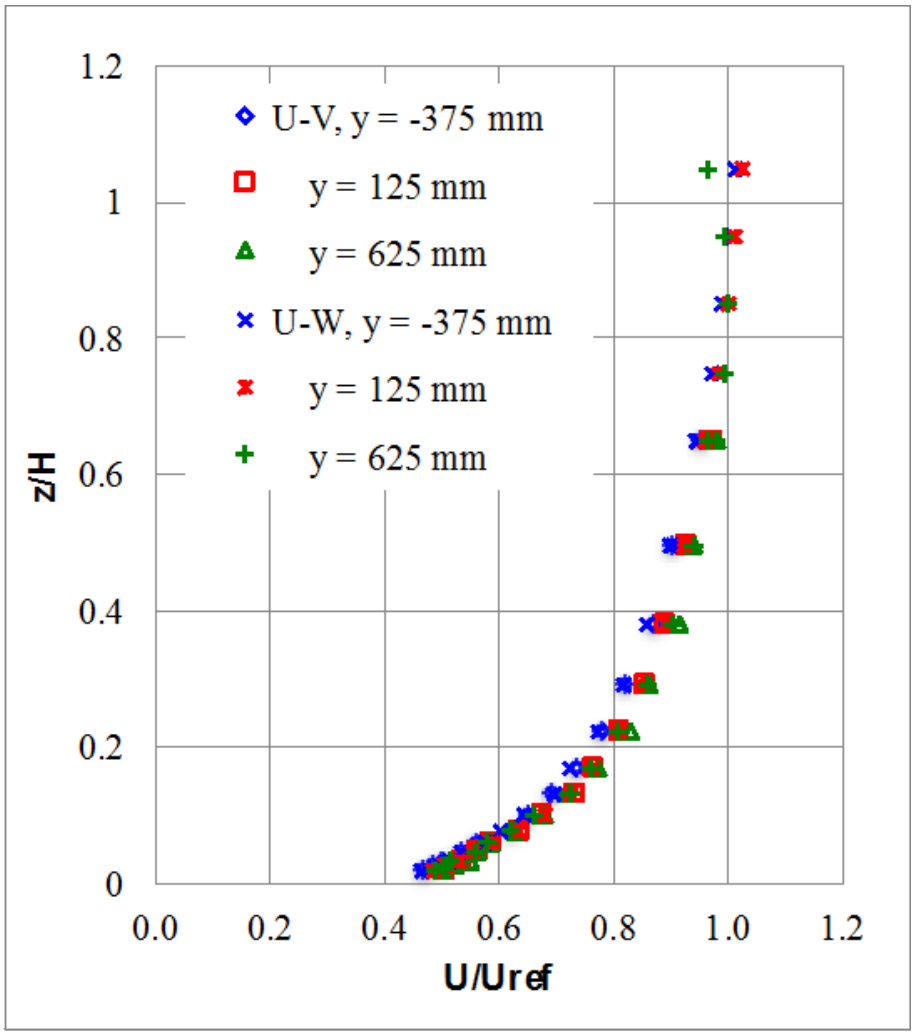

Figure B.1 *Mean velocity profiles at 12.85 m from the working section entrance and three lateral locations measured with the LDA in the $U-V$ and $U-W$ orientations.*

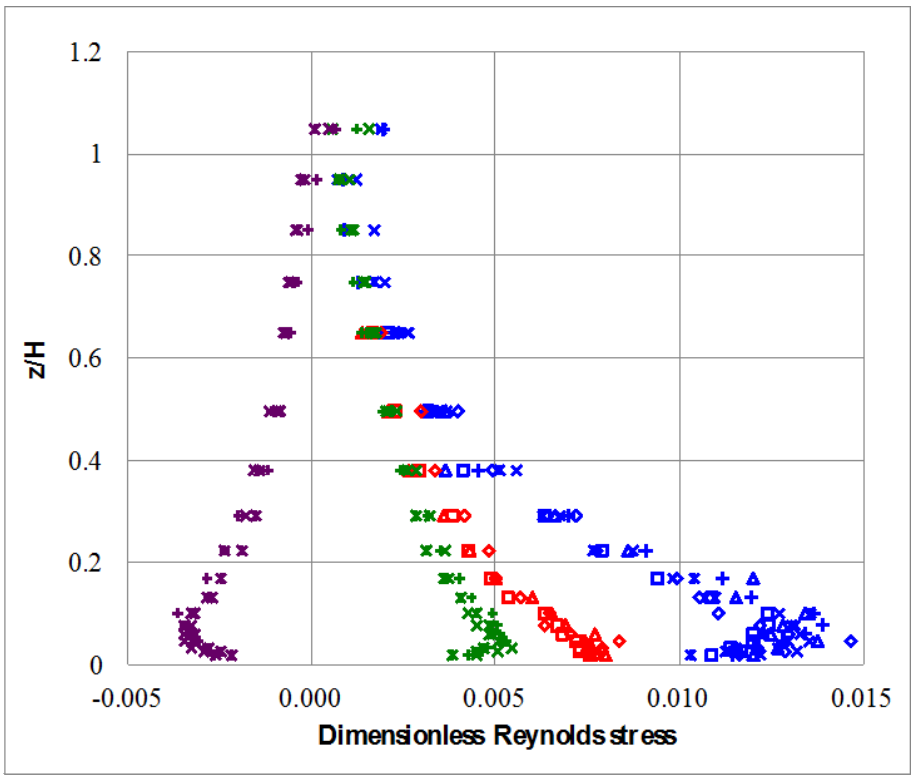

Figure B.2 *Profiles of Reynolds stress (made dimensionless by the reference speed) at 12.85 m from the working section entrance and three lateral positions: blue, u^2; red, v^2; green w^2; purple, uw*

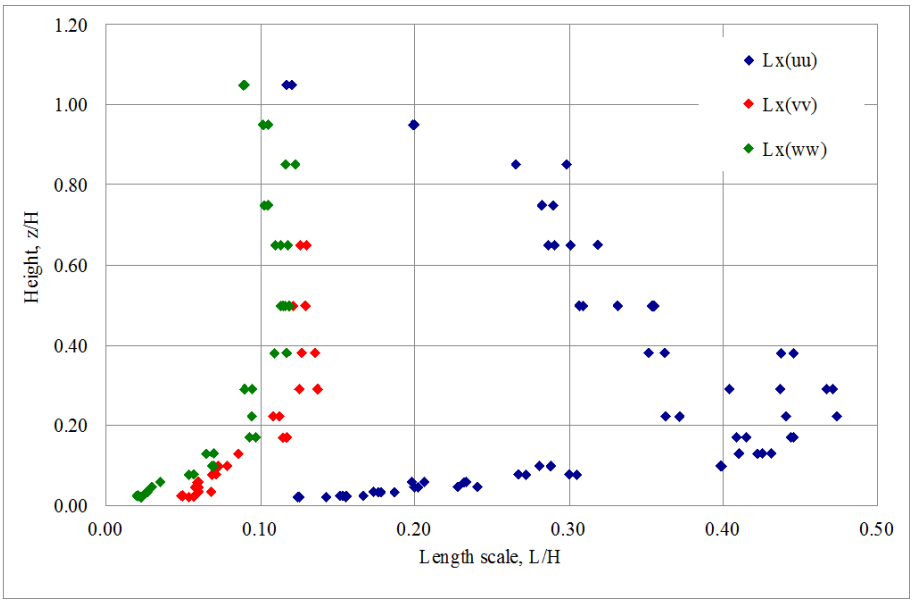

Figure B.3 *Profiles of turbulence length scales (made dimensionless by the boundary layer depth) at 12.85 m from the working section entrance.*

C The hill co-ordinates

A more detailed specification is included in the spreadsheet: 'Wallturb hill coordinates.xlsx'.

x (m)	z (m)	x (m)	z (m)	x (m)	z (m)
0	0	1.049	0.2556	1.999	0.2050
0.048	0.0007	1.097	0.2685	2.047	0.1926
0.099	0.0022	1.149	0.2796	2.099	0.1789
0.147	0.0043	1.197	0.2875	2.147	0.1661
0.199	0.0075	1.248	0.2935	2.198	0.1522
0.247	0.0115	1.300	0.2974	2.250	0.1385
0.298	0.0172	1.348	0.2992	2.298	0.1259
0.350	0.0243	1.377	0.2995	2.349	0.1127
0.398	0.0323	1.377	0.2995	2.397	0.1007
0.449	0.0425	1.399	0.2994	2.449	0.0883
0.497	0.0537	1.447	0.2980	2.496	0.0774
0.549	0.0675	1.499	0.2950	2.548	0.0662
0.596	0.0820	1.546	0.2910	2.600	0.0557
0.648	0.0994	1.598	0.2853	2.647	0.0467
0.700	0.1187	1.650	0.2783	2.699	0.0378
0.747	0.1379	1.697	0.2709	2.747	0.0304
0.799	0.1596	1.749	0.2617	2.798	0.0232
0.847	0.1800	1.797	0.2524	2.850	0.0170
0.898	0.2015	1.848	0.2414	2.898	0.0120
0.950	0.2219	1.900	0.2296	2.949	0.0077
0.998	0.2392	1.948	0.2180	2.997	0.0045

Bibliography

[1] A. Robins, I. Castro, P. Hayden, N. Steggel, D. Contini, and D. Heist, "A wind tunnel study of dense gas dispersion in a neutral boundary layer over a rough surface," Atmospheric environment, vol. 35, no. 13, pp. 2243–2252, 2001.

[2] A. Robins, I. Castro, P. Hayden, N. Steggel, D. Contini, D. Heist, and T. J. Taylor, "A wind tunnel study of dense gas dispersion in a stable boundary layer over a rough surface," Atmospheric Environment, vol. 35, no. 13, pp. 2253–2263, 2001.

[3] C. R. Wood, J. F. Barlow, S. E. Belcher, A. Dobre, S. J. Arnold, A. A. Balogun, J. J. Lingard, R. J. Smalley, J. E. Tate, A. S. Tomlin, et al., "Dispersion experiments in central london: the 2007 dapple project," Bulletin of the American Meteorological Society, vol. 90, no. 7, pp. 955–969, 2009.

[4] A. Rudd, A. G. Robins, J. J. Lepley, and S. E. Belcher, "An inverse method for determining source characteristics for emergency response applications," Boundary-layer meteorology, vol. 144, no. 1, pp. 1–20, 2012.

[5] E. Obasaju and A. Robins, "Simulation of pollution dispersion using small scale physical models-an assessment of scaling options," Environmental Monitoring and Assessment, vol. 52, no. 1-2, pp. 239–254, 1998.

[6] D. J. Hall and S. Walker, "Scaling rules for reduced-scale field releases of hydrogen fluoride," Journal of hazardous materials, vol. 54, no. 1, pp. 89–111, 1997.

[7] W. H. Snyder and I. P. Castro, "The critical reynolds number for rough-wall boundary layers," Journal of Wind Engineering and Industrial Aerodynamics, vol. 90, no. 1, pp. 41–54, 2002.

[8] W. H. Snyder, "Guideline for fluid modeling of atmospheric diffusion," Tech. Rep. EPA-600/8-81-009, Environmental Protection Agency, Research Triangle Park, NC (USA), 1981.

[9] A. Robins and P. Hayden, "The neutral boundary layer in the EnFlo wind tunnel – reference speed, 1 ms^{-1}," Tech. Rep. 4 Rev 1, EnFlo–MODITIC–Note, 3 2014.

[10] G. Briggs, R. Britter, S. Hanna, J. Havens, A. Robins, and W. Snyder, "Dense gas vertical diffusion over rough surfaces: results of wind-tunnel studies," Atmospheric Environment, vol. 35, no. 13, pp. 2265–2284, 2001.

[11] LML, "WALLTURB final report," tech. rep., Laboratoire de Mecanique de Lille, 9 2009.

[12] S. Aubrun and B. Leitl, "Development of an improved physical modelling of a forest area in a wind tunnel," Atmospheric environment, vol. 38, no. 18, pp. 2797–2801, 2004.

About FFI

The Norwegian Defence Research Establishment (FFI) was founded 11th of April 1946. It is organised as an administrative agency subordinate to the Ministry of Defence.

FFI's MISSION

FFI is the prime institution responsible for defence related research in Norway. Its principal mission is to carry out research and development to meet the requirements of the Armed Forces. FFI has the role of chief adviser to the political and military leadership. In particular, the institute shall focus on aspects of the development in science and technology that can influence our security policy or defence planning.

FFI's VISION

FFI turns knowledge and ideas into an efficient defence.

FFI's CHARACTERISTICS

Creative, daring, broad-minded and responsible.

Om FFI

Forsvarets forskningsinstitutt ble etablert 11. april 1946. Instituttet er organisert som et forvaltningsorgan med særskilte fullmakter underlagt Forsvarsdepartementet.

FFIs FORMÅL

Forsvarets forskningsinstitutt er Forsvarets sentrale forskningsinstitusjon og har som formål å drive forskning og utvikling for Forsvarets behov. Videre er FFI rådgiver overfor Forsvarets strategiske ledelse. Spesielt skal instituttet følge opp trekk ved vitenskapelig og militærteknisk utvikling som kan påvirke forutsetningene for sikkerhetspolitikken eller forsvarsplanleggingen.

FFIs VISJON

FFI gjør kunnskap og ideer til et effektivt forsvar.

FFIs VERDIER

Skapende, drivende, vidsynt og ansvarlig.

FFI's organisation

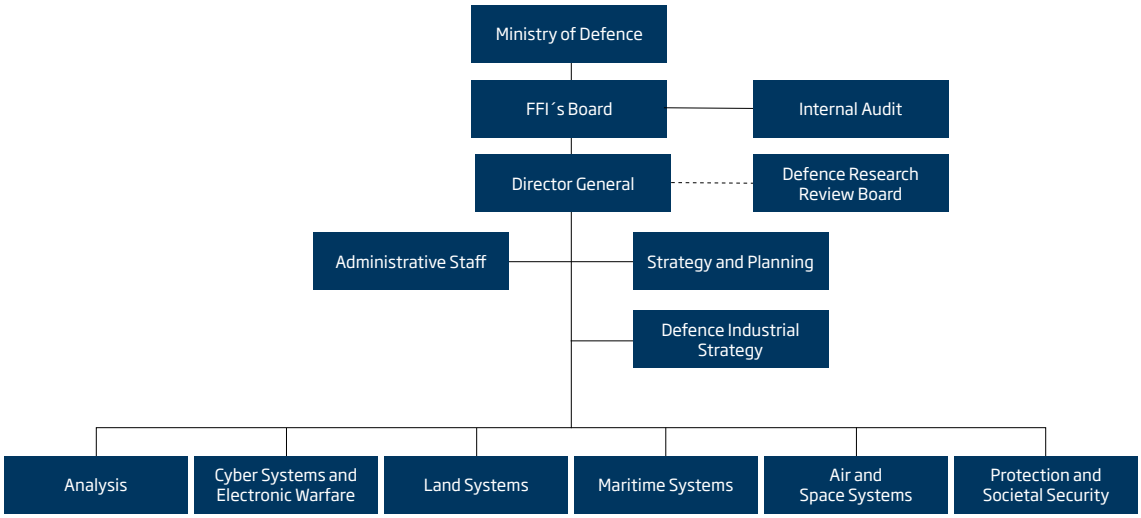

Forsvarets forskningsinstitutt
Postboks 25
2027 Kjeller

Besøksadresse:
Instituttveien 20
2007 Kjeller

Telefon: 63 80 70 00
Telefaks: 63 80 71 15
Epost: ffi@ffi.no

Norwegian Defence Research Establishment (FFI)
P.O. Box 25
NO-2027 Kjeller

Office address:
Instituttveien 20
N-2007 Kjeller

Telephone: +47 63 80 70 00
Telefax: +47 63 80 71 15
Email: ffi@ffi.no

FFI Forsvarets forskningsinstitutt
Norwegian Defence Research Establishment